Supporting Materials

Solvothermal Sulfurization in Deep Eutectic Solvent: A Novel Route to Synthesize Co-doped Ni_3S_2 Nanosheets Supported on Ni foam as Active Materials for Ultrahigh-Performance Pseudocapacitors

J.R. Zeng,[a] L. Chen,[a] S.S. Siwal,[a] Q.B. Zhang[a,b*]

[a] Key Laboratory of Ionic Liquids Metallurgy, Faculty of Metallurgical and Energy Engineering, Kunming University of Science and Technology, Kunming, 650093, P.R. China

[b] State Key Laboratory of Complex Nonferrous Metal Resources Cleaning Utilization in Yunnan Province, Kunming 650093, P.R.

*Corresponding author. Tel: +86-871-65162008; Fax: +86-871-65161278.

E-mail address: qibozhang@kmust.edu.cn (Q.B. Zhang)

Experimental section

Chemicals and Materials: Choline chloride (ChCl, $HOC_2H_4N(CH_3)_3Cl$), ethylene glycol (EG,C_2H_5OH), thiourea (TU, CH_4N_2S), nickel chloride hexahydrate ($NiCl_2{\cdot}6H_2O$), cobalt chloride hexahydrate ($CoCl_2{\cdot}6H_2O$), potassium hydroxide (KOH),and hydrochloric acid (HCl) were purchased from Aladdin Ltd. (Shanghai China). All the chemicals used are of analytical purity and used without further purification. The DES, Ethaline used in this study was a 1:2 molar ratio of ChCl and EG, which were stirred at 343 K until a homogeneous solution was obtained. Polyvinylidene fluoride (PVDF, KYNAR HSV 900 PWD), active carbon (AC, YEC-800), separator (NKK-MPF30AC-100), acetylene black and N-methyl-2-pyrrolidone (NMP, C5H9NO) were purchased from Tianjin EVS chemicals Science and Technology Ltd., China.

Synthesis of Co-Ni_3S_2/NF: Firstly, the NF with a geometric dimension of 1.0 cm × 3.0 cm ×1.5 mm was soaked in 3 M HCl for 20 min with ultrasonication to remove the surface oxide layer and cleaned in ethanol and deionized (DI) water. Then 0.50 M $NiCl_2{\cdot}6H_2O$ and 0.30 M $CoCl_2{\cdot}6H_2O$ (as a Ni-Co precursor) were dissolved in 40 mL Ethaline under vigorous stirring for 30 min. A typical three-electrode cell at 333 K uses to the deposition of Ni-Co on NF; the NF, two parallel-arranged graphite sheets, and an Ag/Ag^+ (filling with 0.01 M AgCl/Ethaline) as the working, counter and the reference electrode, respectively. The deposition potential was carried out at -0.80 V vs. Ag/Ag^+ based on the cyclic voltammogram (CV) investigations as shown in Fig. S1, with an optimized charge density of 100 C cm^{-2}. After deposition, the Ni-Co/NF was taken out and washed with DI water before vacuum dried. Subsequently, the deposition obtained Ni-Co/NF was immersed into Ethaline containing 0.05 M TU at 353 K for sulfurization within 5 h under a standard atmosphere, and then naturally cooled to obtain Co-Ni_3S_2/NF. Finally cooling down naturally, the as-obtained samples were washed by acetone and deionized water several times in order to remove the residuals. For comparison, the samples of pure deposited Ni and Ni-Co on NF were also prepared (denoted as pure Ni/NF and Ni-Co/NF, respectively) without sulfurization.

Assembling of Co-Ni_3S_2/NF//AC asymmetric supercapacitor (ASC) device: 6 g PVA and 3 g KOH were added into 60 ml DI water and mixed well at a 363 K to get the gel electrolyte (PVA/KOH). The AC electrode was prepared by mixing 80 wt.% AC and 10 wt.% acetylene black

with 10 wt.% PVDF, and it is well-grinded in an agate mortar for about 20 min by adding a proper amount of NMP solvent. Then the mixture material was painted onto the surface of a clean NF according to the matched weight. As for fabrication of an asymmetric supercapacitor (ASC) device (1.0 cm × 2.0 cm ×2 mm), Co-Ni_3S_2/NF as the positive and AC as the negative electrode with a separator (NKK-MPF30AC-100) sandwiched between the two electrodes. Finally, the assembled electrodes were dried overnight at room temperature.

Materials Characterization: X-ray diffraction (XRD) patterns were acquired on a Rigaku Minifex‖ Desktop diffractometer with Cu Kα radiation. The specific surface area and pore size distribution of the samples were evaluated by a Micromeritics ASAP 2020 system at liquid N_2 temperature based on the Barrett-Joyner-Halenda model. X-ray photoelectron (XPS) was conducted on an X-ray photoelectron spectroscopy (XPS, PHI 550) to character the surface chemical states of the samples. Scanning electron microscopy (SEM) and energy-dispersive X-ray spectrum (EDX) measurements were recorded on a NOVA NanoSEM 450 scanning electron microscope equipped with EDX system at an accelerating voltage of 15 kV. Transmission electron microscopy (TEM) measurements were taken on a Tecnai G2 F30 electron microscopy with an accelerating voltage 200 kV. The element contents of the samples were analyzed by inductively coupled plasma mass spectroscopy (ICP-MS, Perkin-Elmer Elan DRC-e, USA).

Electrochemical Measurement: Various electrochemical measurement techniques based on a three-electrode configuration were performed on a CHI 760D electrochemical workstation using a 1.0 M KOH solution as the electrolyte at room temperature. The fabricated Co-Ni_3S_2/NF electrode was served as the working electrode with an Hg/HgO (filing with 1 M KOH) as the reference electrode and a Pt rod (Φ2 mm) as the counter electrode. Cycle voltammetry (CV) measurements were carried out at various scan rates ranging from 5 to 100 mV s^{-1} with a potential range of 0-0.80 V vs. Hg/HgO. Galvanostatic charge and discharge (GCD) curves were measured at various current densities of 5, 10, 20, 30, and 40 mA cm^{-2} with the potential window between 0 and 0.60 V vs. Hg/HgO.

The areal specific capacitance C_s (F cm^{-2}) and mass specific capacitance C_m (F g^{-1}) were calculated by following formulae[1]:

$$C_s = \frac{i \times \Delta t}{S \times \Delta V}$$

$$C_m = \frac{i \times \Delta t}{m \times \Delta V}$$

where i is the constant discharge current, Δt (s) is the discharge time, S (cm^{-2}) is the geometrical area of the electrode, m (g) is the mass loading of the active electrode material, and ΔV is the potential drop upon discharging.

The specific capacitance based on CV results was used the following formula[2]:

$$C = \frac{\int I(V)dV}{S\Delta v(V_2 - V_1)}$$

Where C (mF cm^{-2}) is the specific capacitance, I (V) (mA cm^{-2}) is the instantaneous current, $\int I(V)dV$ (C) is total voltametric charge, Δv (mV s^{-1}) is the scan rate, S (cm^{-2}) is the geometrical area of the electrode, and $(V_2 - V_1)$(V) is the potential window.

In the two-electrode (full cell) ASC system, Co-Ni_3S_2/NF and active carbon coated on NF (AC/NF) were served as the cathode and anode, respectively. To balance the charges on both electrodes, the ASC should follow the relationship $Q^+ = Q^-$, and the mass ratio of the positive electrode to the negative electrode was optimized by using the following formulae[3]:

$$\frac{m^+}{m^-} = \frac{Q^-}{Q^+}$$

$$Q = C_m \times m \times \Delta V$$

Where m^+ and m^- are mass loadings of the positive and negative electrode, respectively. Q^+ and Q^- are the charge of the positive and negative electrode, respectively. C_s and ΔV are the specific capacitance and potential window. The mass loading of the active Co-Ni_3S_2/NF is about 0.428 mg cm^{-2} based on the ICP-MS result (Table S1). Moreover, the corresponding mass loading of AC/NF is 1.1 mg cm^{-2}. The electrochemical performance of the assembled ASC device was also investigated based on the two-electrode system. Electrochemical impedance spectroscopy (EIS) measurements were obtained at an open circuit potential in the frequency range from 0.1 Hz to 100 kHz with an AC potential amplitude of 5 mV.

The cell specific capacitance C_{cell} (F g^{-1}), energy density E (Wh kg^{-1}), and power density P (kW kg^{-1}) of the assembled ASC device were obtained using the following formulae[1]:

$$C_{cell} = \frac{i \times \Delta t}{M \times \Delta V}$$

$$E = \frac{1}{2} \frac{C_{cell} \Delta V^2}{3.6}$$

$$P = 3600 \times \frac{E}{\Delta t}$$

Where M (g) is the total mass weight of the active materials supported on negative and positive electrodes, ΔV is the voltage applied during the charging/discharging process, and t_d (s) refers to the discharge time.

According to the battery-type behavior of the Co-Ni_3S_2/NF, the specific capacity (Q) was calculated from the GCD plots based on following formulae[4]:

$$Q_m = \frac{i \times \Delta t}{m}$$

$$Q_s = \frac{i \times \Delta t}{S}$$

Where Q_m (mAh g^{-1}) represents the specific capacity and Q_s (mAh cm^{-2}) is the areal capacity, i (A) is the discharge current, Δt (h) is the discharge time, S is the mass loading, and m is the area of the active materials.

The energy density E (Wh kg^{-1}) and power density P (kW kg^{-1}) of battery-type device was calculate by following formulae[5]:

$$E = \int_{t_1}^{t_2} (i \times V) dt$$

$$P = E/\Delta t$$

Where V is the voltage, t_1 and t_2 is the start time and end time during discharging and Δt equal to (t_2-t_1) represents the discharge time.

DFT Calculation details: All calculations are performed based on spin-polarized density functional theory (DFT) using the Material studio 8.0 of Accelry Inc. The general gradient approximation (GGA) parametrized by Perdew, burke, and Ernzerhof (PBE) is used as the exchange-correlation functional, and the projector augmented-wave (PAW) method is used to describe the ion-electro interaction. A kinetic energy cutoff 400 eV is used for the plan-wave basis, and the Brillouin zone is sampled in k-space using a Monkhorst-Pack scheme of 2×2×2. The force and energy convergence criterion is set to 0.01 eV /Å and 10^{-5} eV, respectively. Moreover, 1×1×1 k-point grid was used to calculate the DOS. The free energies of the

intermediates were calculated at 298 K, and (001) surface with a vacuum layer of 15 Å was selected. The adsorption energy of intermediates (OH^-) on substrate followed the approach of Nøeskov et al.[6], and the energy calculated by the following equation:

$$\Delta E_{(OH)} = E_{(OH/surf)} - [E_{(surf)} + E_{(H_2O)} - \frac{1}{2}E_{(H_2)}]$$

where $E_{(OH/surf)}$ represent the total energies of OH^- on substrate, $E_{(surf)}$, $E_{(H_2O)}$, and $E_{(H_2)}$ are the total energies of bare substrate, water, and hydrogen gas, respectively.

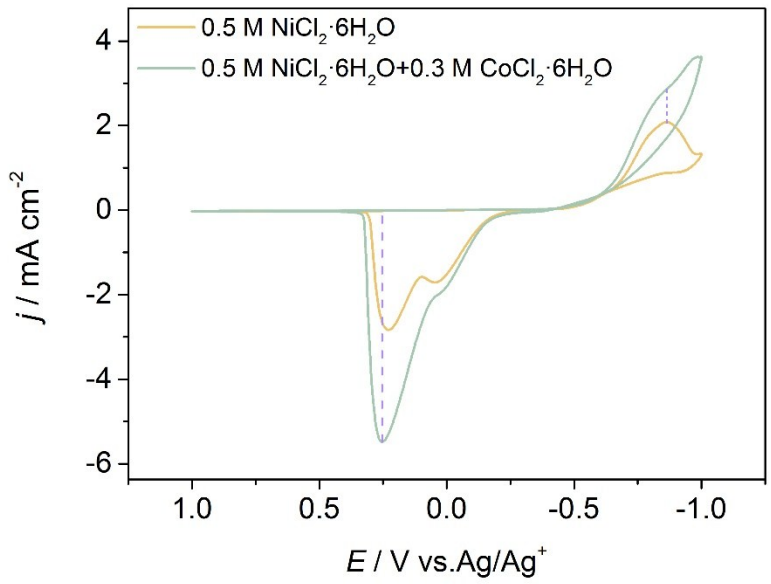

Fig. S1. CV curves of Ethaline containing 0.5 M $NiCl_2 \cdot 6H_2O$ without and with 0.3 M $CoCl_2 \cdot 6H_2O$.

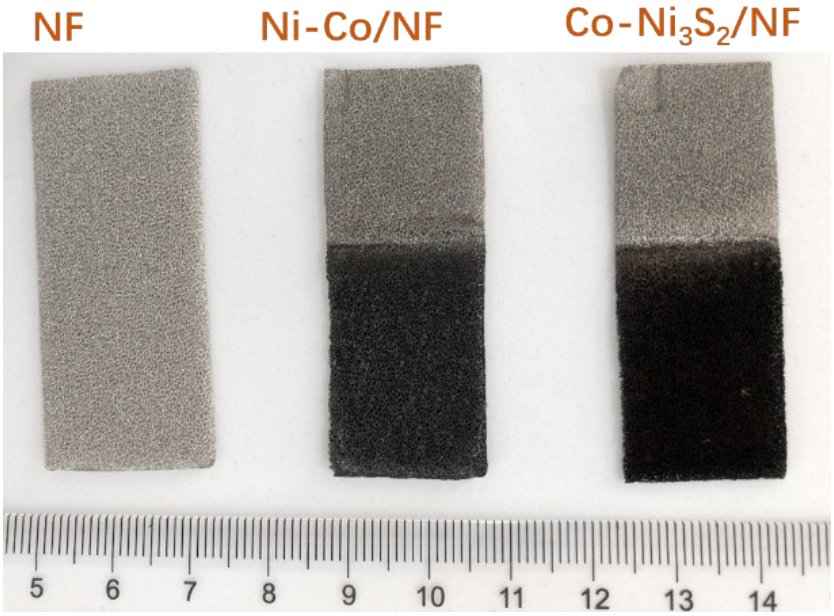

Fig. S2. The photo images of NF, Ni-Co/NF and Co-Ni_3S_2/NF.

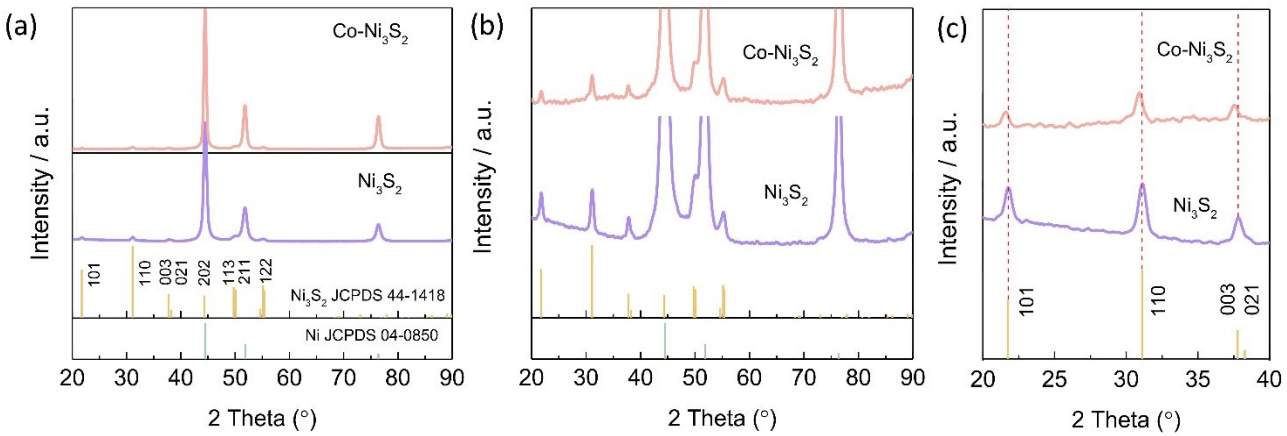

Fig. S3. (a) The powder XRD patterns of as-prepared Co-Ni_3S_2 and Ni_3S_2, (b) shows the corresponding curves after extending the y-axis to more clear the peak intensity. (c) The typical shift after Co doping in the enlarged range of 20°-40°.

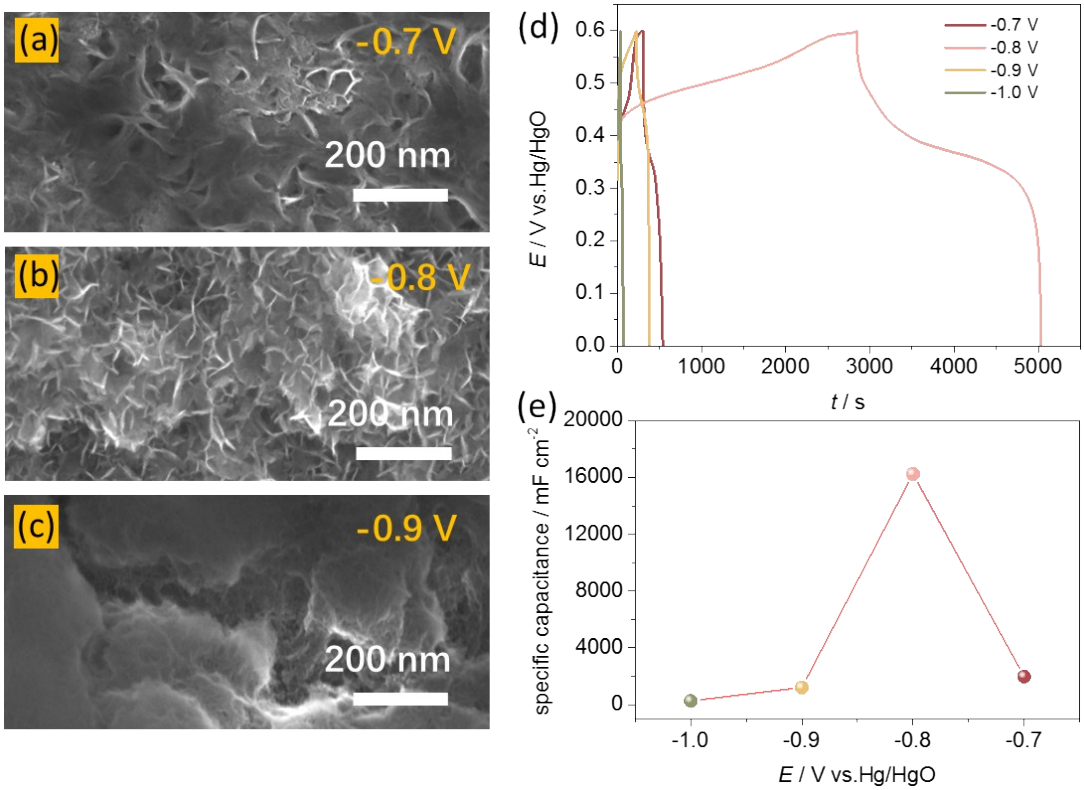

Fig. S4. (a-c) SEM images of Co-Ni_3S_2/NF electrodes obtained at different applied potentials (as indicated). (d) The GCD curves of each prepared Co-Ni_3S_2/NF electrodes, and (e) the corresponding specific capacitance. The Ni-Co/NF electrodes were electrodeposited in Ethaline containing 0.5 M $NiCl_2{\cdot}6H_2O$ and 0.3 M $CoCl_2{\cdot}6H_2O$ under different potentials (from -0.7 to -1.0 V vs. Ag/Ag^+) with a charge density of 100 C cm^{-2}, followed by sulfurization in Ethaline containing 0.03 M TU for 3h at 353 K to obtain Co-Ni_3S_2/NF electrodes.

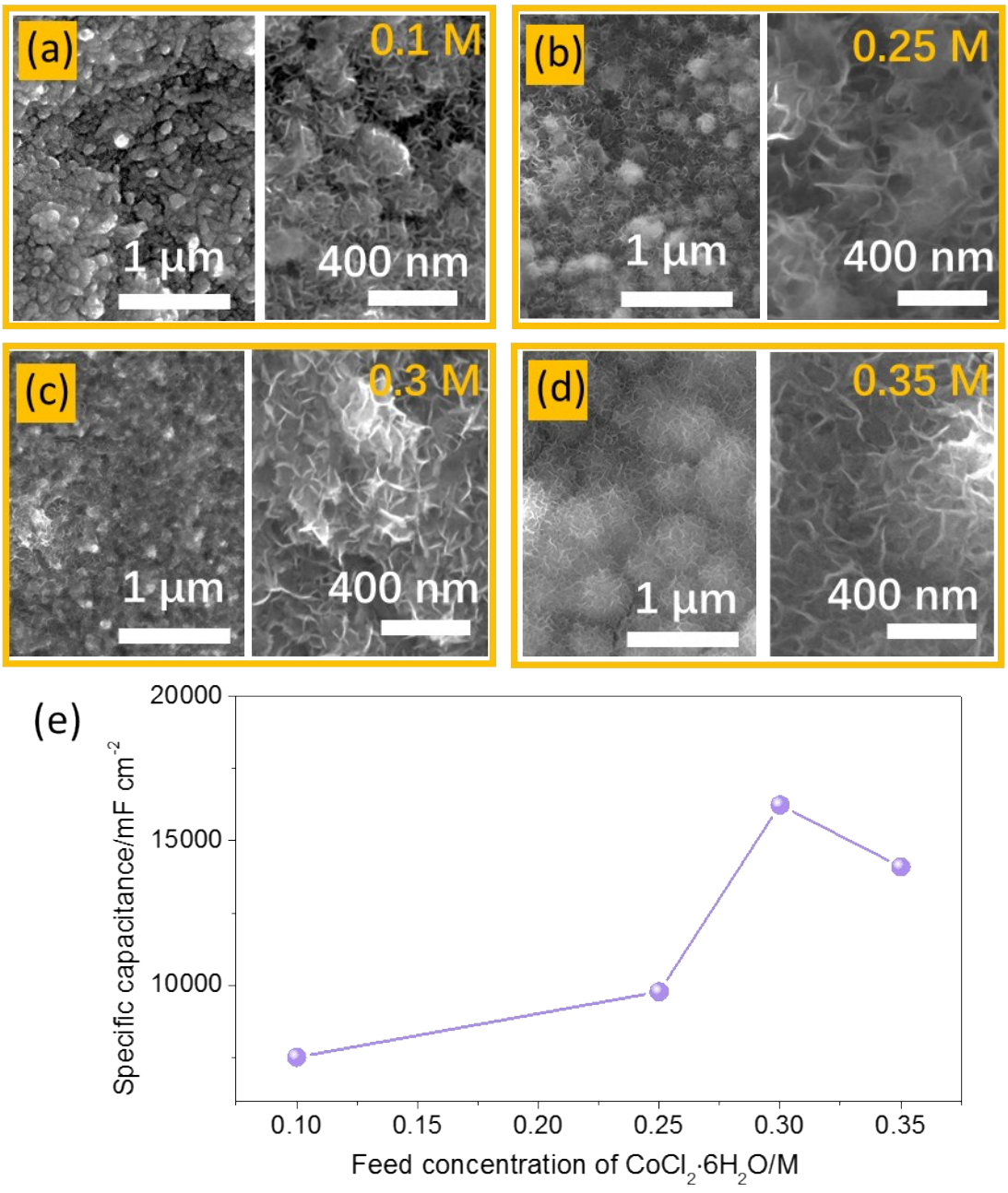

Fig. S5. SEM images of Co-Ni_3S_2/NF with different feed concentrations of $CoCl_2 \cdot 6H_2O$: (a) 0.1M, (b) 0.25 M, (c) 0.3 M, and (d) 0.35 M. (e) The corresponding specific capacitance. The Ni-Co/NF electrodes were prepared by electrodepositing in Ethaline containing 0.5 M $NiCl_2 \cdot 6H_2O$ with different feed concentrations of $CoCl_2 \cdot 6H_2O$ under the potential of -0.80 V vs. Ag/Ag^+ with a charge density of 100 C cm^{-2}, followed by sulfurization in Ethaline containing 0.03 M TU for 3h at 353 K to obtain Co-Ni_3S_2/NF electrodes.

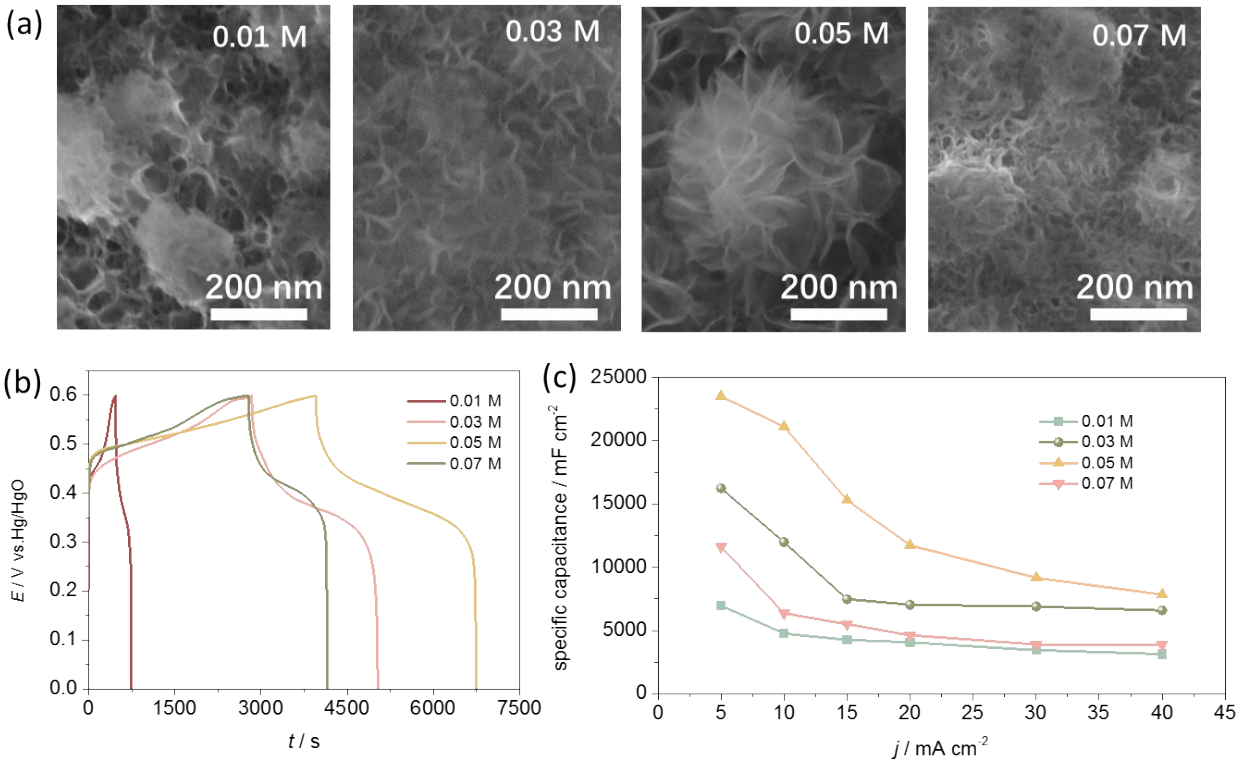

Fig. S6. (a) SEM images of Co-Ni_3S_2/NF electrodes obtained with Ni-Co/NF precursor for sulfurization at 353 K in Ethaline containing different concentrations of TU (the sulfurization time is 5 h). (b) The GCD curves of Co-Ni_3S_2/NF sulfurized at different TU concentrations. (c) The corresponding liner graph shows the specific capacitance. (The Ni-Co electrode was prepared under the potential of -0.8 V vs. Ag/Ag^+ with a charge density of 100 C cm^{-2} in Ethaline contain 0.5 M $NiCl_2 \cdot H_2O$ and 0.3 M $CoCl_2 \cdot H_2O$).

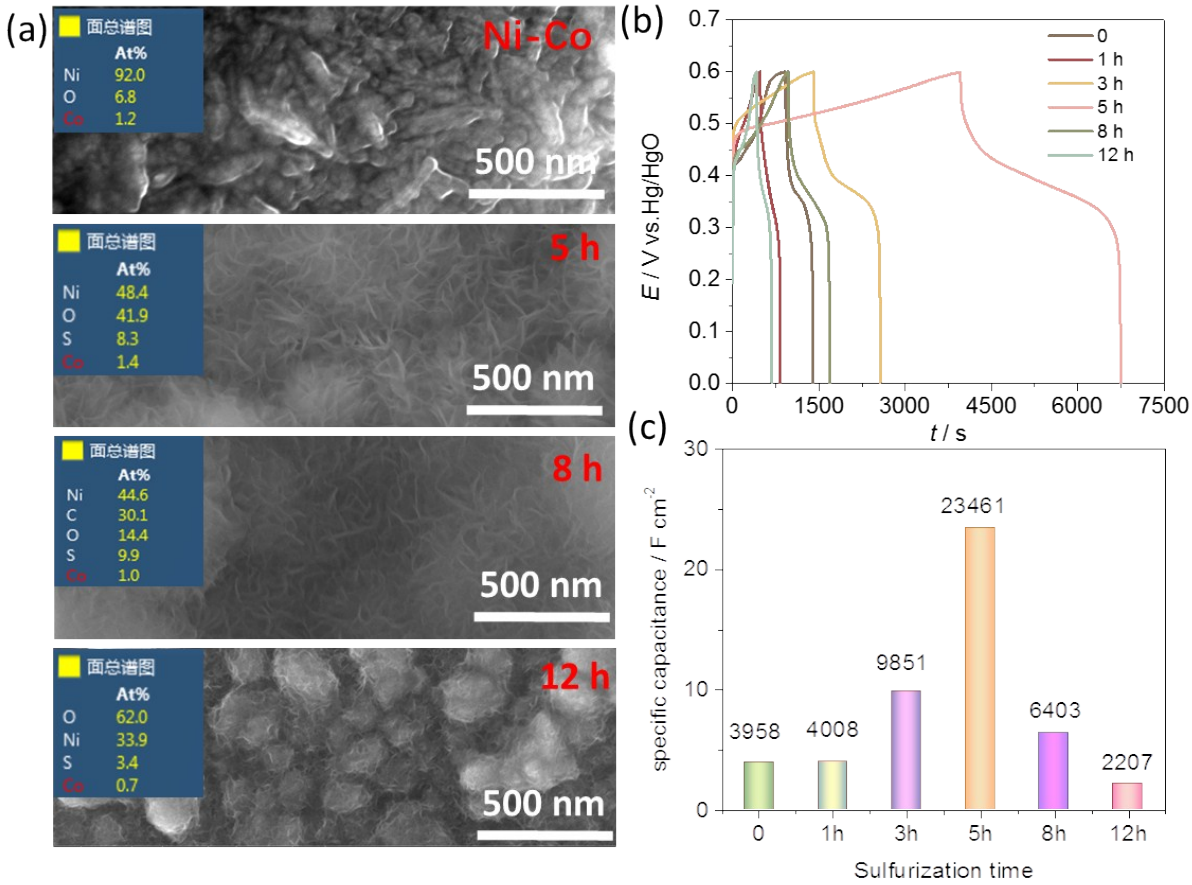

Fig. S7. (a) SEM images of Ni-Co/NF and Co-Ni_3S_2/NF electrodes synthesized at different sulfurization time: 0 h, 5h, 8 h, and 12 h. (b) The corresponding GCD curves and (c) specific capacitances of the Co-Ni_3S_2/NF electrodes. The Ni-Co/NF electrodes were obtained from Ethaline containing 0.5 M $NiCl_2{\cdot}6H_2O$ and 0.3 M $CoCl_2{\cdot}6H_2O$ at -0.8 V vs. Ag/Ag^+ with a charge density of 100 C cm^{-2}, followed by sulfurization at 353 K in Ethaline with 0.05 M TU for different time to obtain Co-Ni_3S_2/NF electrodes.

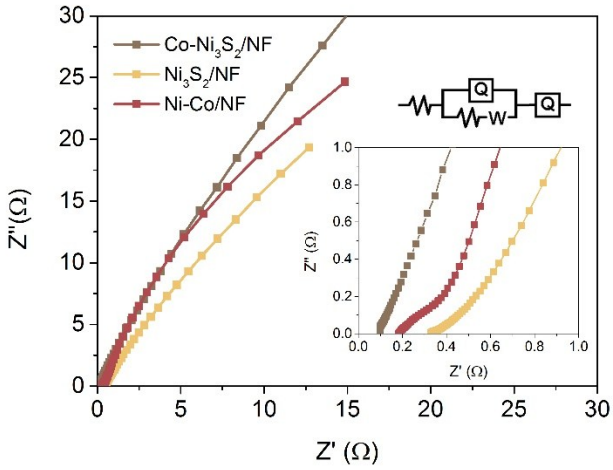

Fig. S8 Nyquist plots of Co-Ni_3S_2/NF, Ni_3S_2/NF and Ni-Co/NF. Inset: expanded views of the high frequency region and the equivalent circuit diagram used for fitting the impedance spectra in the upper part.

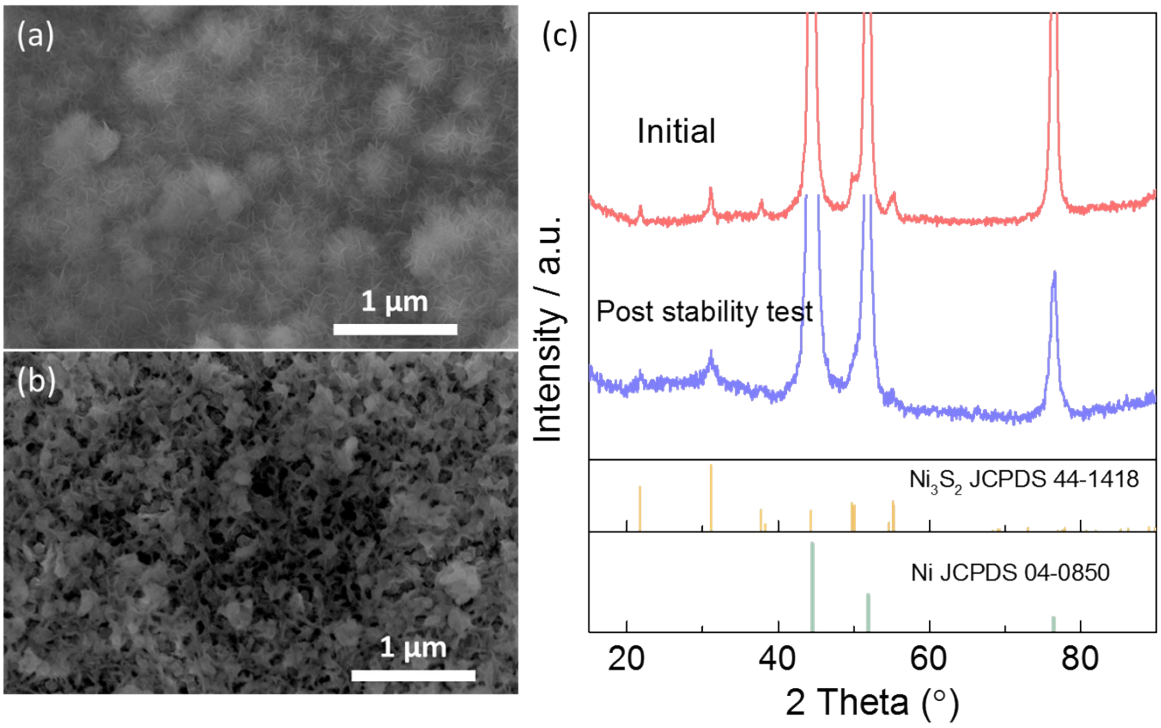

Fig. S9. SEM images of Co-Ni_3S_2/NF (a) before and (b) after long-term cycling stability test. (c) Powder XRD patterns of Co-Ni_3S_2 before and after long-term cycling stability test.

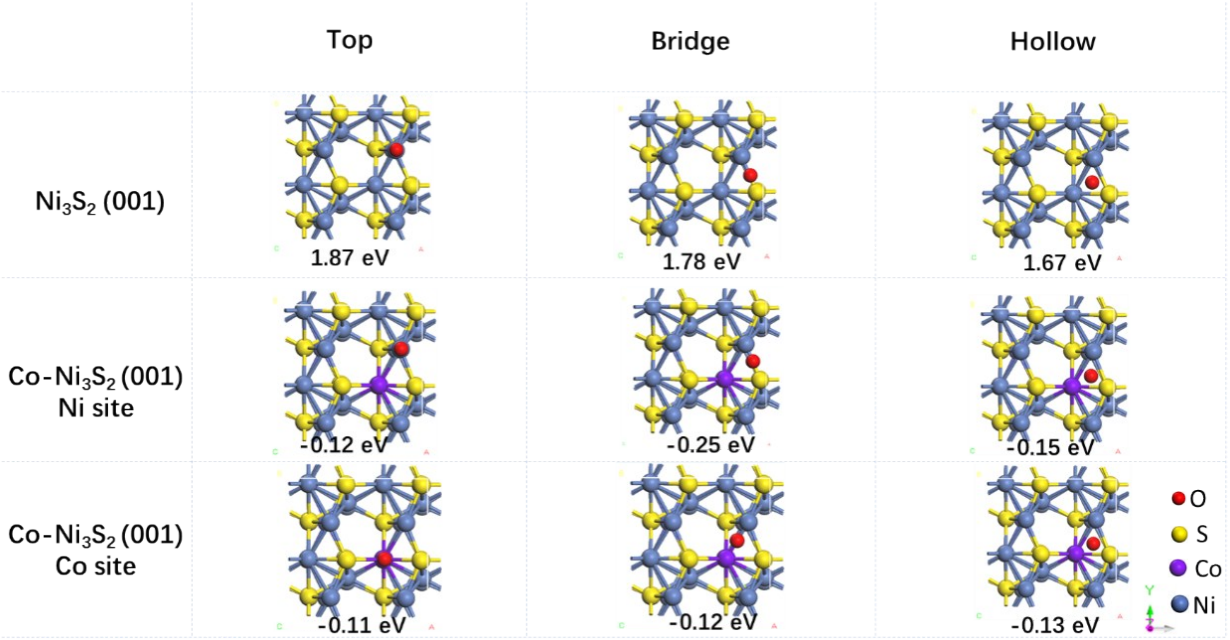

Fig. S10. Calculated adsorption energies of OH^- on Ni_3S_2 (001) and Co-Ni_3S_2 (001) with Ni- and Co-sites.

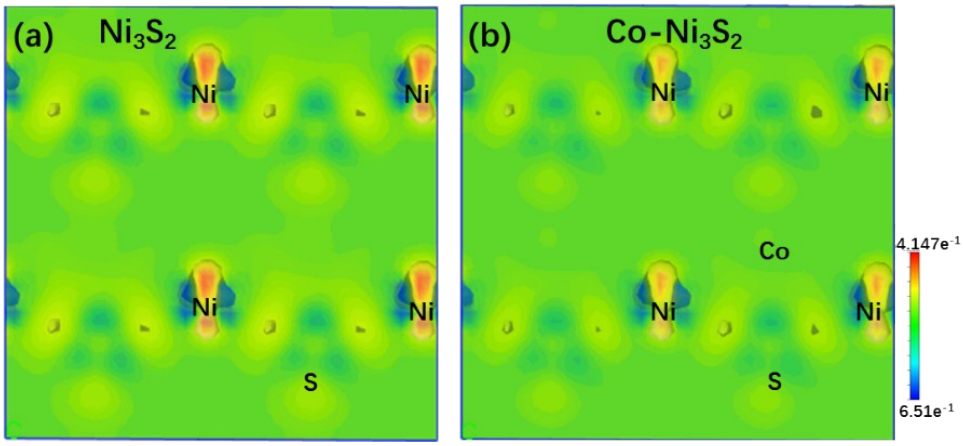

Fig. S11. The top view difference charge density of (a) Ni_3S_2 (001), and (b) Co-Ni_3S_2 (001).

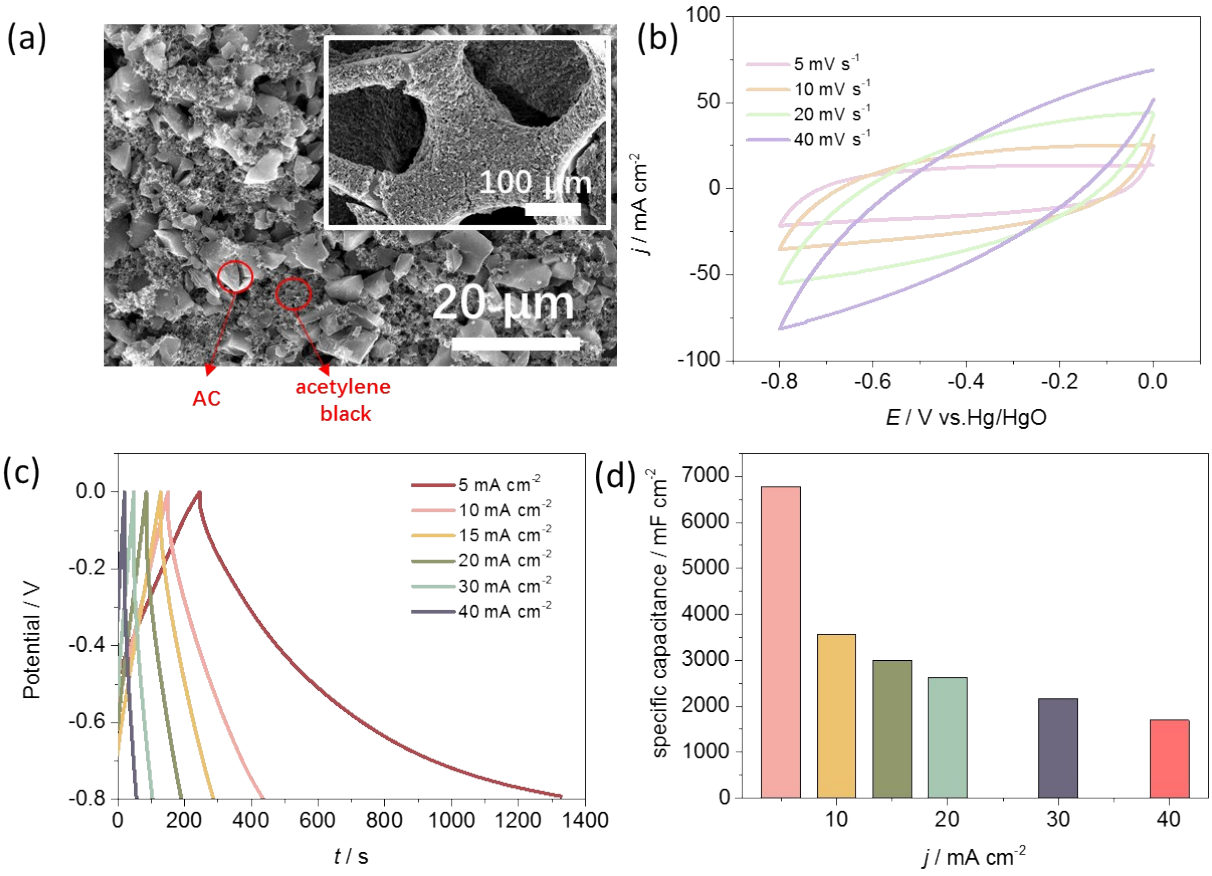

Fig. S12. (a) SEM image of AC/NF particles. (b) CV curves of AC/NF with different scan rates from 5 to 100 mV s^{-1}. (c) GCD curves and (d) specific capacitances of AC/NF at different current densities.

Fig. S12a shows the SEM image of AC particles that are well-distributed on NF. In Fig. S12b, the CV curves exhibit nearly rectangular shapes, clearly indicating the typical EDLC behavior of the AC/NF. Fig. S12c displays that the GCD curves of the AC/NF measured at various current densities are approximately symmetric, which suggest that the AC/NF electrode is reversible. The specific capacitance of AC/NF is shown in Fig. S12d. The areal specific capacitance can reach 6787 mF cm^{-2} at a current density of 5 mA cm^{-2}. To balance the charge on both electrodes, the mass ratio of the positive electrode (Co-Ni_3S_2/NF) to the negative electrode (AC/NF) is optimized using this formula: $m^+/m^-=Q^+/Q^-$ (The more calculation details are shown in experiment section).

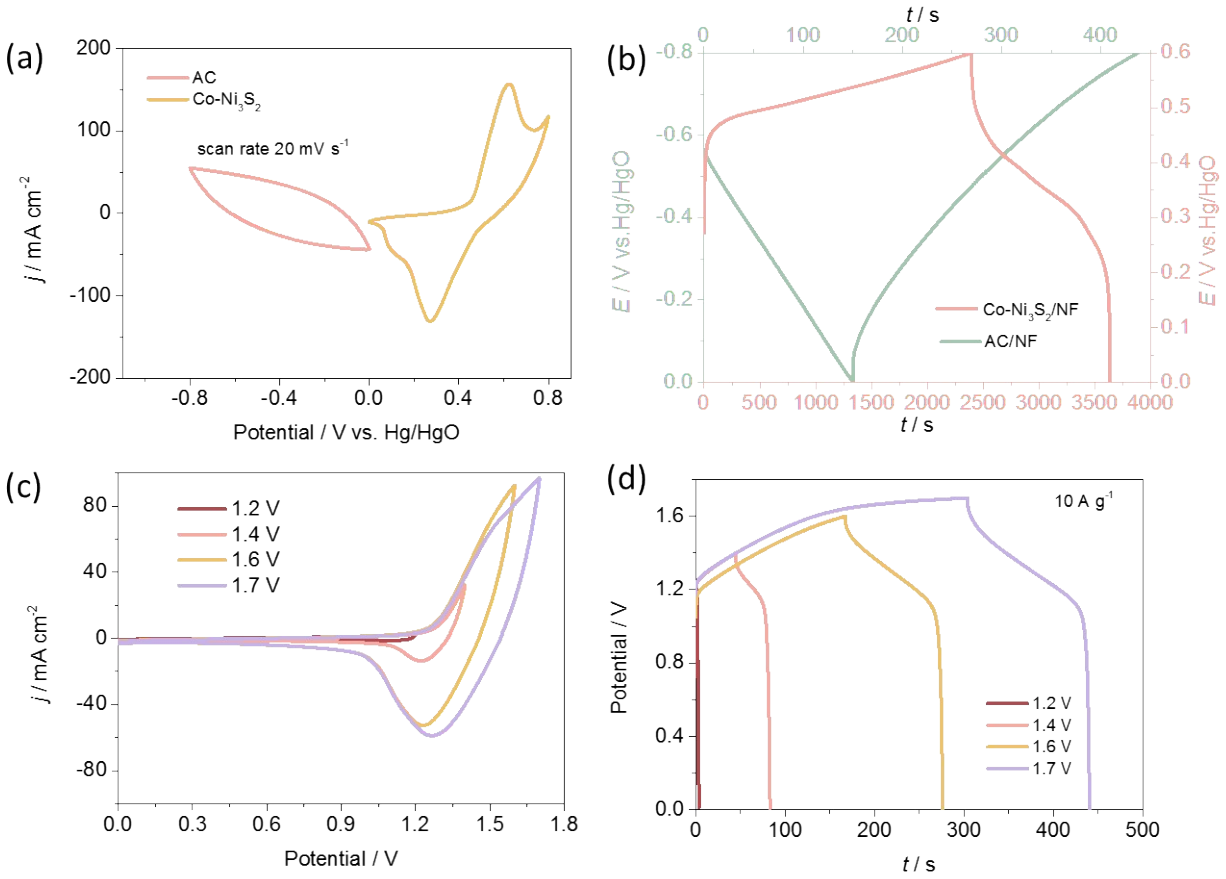

Fig. S13. (a) The CV curves of Co-Ni_3S_2 and AC/NF in a three-electrode system with a Hg/HgO as reference electrode at a scan rate of 20 mV s^{-1}. (b) The GCD curves of Co-Ni_3S_2 and AC/NF at a current density of 10 mA cm^{-2}. (c) The CV and (d) GCD curves of Co-Ni_3S_2/NF//AC/NF device at different potential windows.

Table S1. The relative contents of elements in Co-Ni_3S_2/NF derived from ICP-MS.

Element	Mass loading (mg cm^{-2})	
	Initial	Post 3000 cycle stability test
Ni	0.297	0.261
Co	0.023	0.019
S	0.108	0.103
Ni:Co(At%)	11.8:1	13.5:1

Table S2. The R_{ct} and R_s values of Co-Ni_3S_2/NF, Ni_3S_2/NF and Ni-Co/NF.

Electrode	R_{ct} (Ω)	R_s (Ω)
Co-Ni_3S_2/NF	0.51	0.09
Ni_3S_2/NF	1.86	0.31
Ni-Co/NF	0.56	0.19

Table S3. Comparison of the electrochemical performance of our Co-Ni_3S_2/NF with some other previously reported ternary nickel cobalt sulfides based electrode materials in a three-electrode system.

Electrode	Current collector	Electrolyte	Mass loading (mg cm^2)	Current density	Specific capacitance	Areal capacity	Refs
Co-Ni_3S_2/NF	NF	1M KOH	0.428	5 mA cm^{-2}	23491 mF cm^{-2}	3915 μAh cm^{-2}	**This work**
				10 mA cm^{-2}	20817 mF cm^{-2}	3470 μAh cm^{-2}	
				15 mA cm^{-2}	18000 mF cm^{-2}	3001 μAh cm^{-2}	
				20 mA cm^{-2}	11533 mF cm^{-2}	1922 μAh cm^{-2}	
				30 mA cm^{-2}	7850 mF cm^{-2}	1308 μAh cm^{-2}	
				40 mA cm^{-2}	7000 mF cm^{-2}	1167 μAh cm^{-2}	
Co doped Ni_3S_2@CNT	Graphite foam (GNF)	6 M KOH	4	1 mA cm^{-2}	4.1 F cm^{-2}		7
				5 mA cm^{-2}	3.8 F cm^{-2}		
				10 mA cm^{-2}	3.5 F cm^{-2}		
				40 mA cm^{-2}	2.4 F cm^{-2}		
$NiCo_2S_4$	Carbon Fiber Paper	1M KOH	4.3	20 mA cm^{-2}	0.58 F cm^{-2}		8
				4 mA cm^{-2}	0.87F cm^{-2}		
$CoNi_2S_4$ nanocomposite	graphene	3 M KOH	--	1 A g^{-1}	2099.1 F g^{-1}		9
				2 A g^{-1}	1961.6 F g^{-1}		
				3 A g^{-1}	1843.7 F g^{-1}		
				4 A g^{-1}	1737.5 F g^{-1}		
				5 A g^{-1}	1651.7 F g^{-1}		
$NiCo_2S_4$ microparticles	NF	6 M KOH	4	3A g^{-1}	1048 F g^{-1}		10
				4A g^{-1}	868 F g^{-1}		
				6A g^{-1}	750 F g^{-1}		
				8A g^{-1}	620 F g^{-1}		
				10A g^{-1}	525 F g^{-1}		
$NiCo_2S_4$@CoS_x nanotube	NF	1 M KOH	2.78	5 mA cm^{-2}	4.74 F cm^{-2}		11
				10 mA cm^{-2}	4.41 F cm^{-2}		
				15 mA cm^{-2}	4.09 F cm^{-2}		
				20 mA cm^{-2}	3.76 F cm^{-2}		
				25 mA cm^{-2}	3.48 F cm^{-2}		
				50 mA cm^{-2}	2.26 F cm^{-2}		
CoS@$NiCo_2S_4$ NWSAs	NF	2 M KOH	2.35	5 mA cm^{-2}	7.62 F cm^{-2}		12
				10 mA cm^{-2}	7.06 F cm^{-2}		
				15 mA cm^{-2}	6.54 F cm^{-2}		
				20 mA cm^{-2}	6.16 F cm^{-2}		

				25 mA cm^{-2}	5.82 F cm^{-2}	
				30 mA cm^{-2}	5.52 F cm^{-2}	
$NiCo_2S_4$ nanoparticles	NF	2 M KOH	--	3 A g^{-1}	1440 F g^{-1}	13
$NiCo_2S_4$ hexagonal plates	NF	2 M KOH	3-4	0.5 A g^{-1}	998.9 F g^{-1}	14
				1 A g^{-1}	966.5 F g^{-1}	
				2 A g^{-1}	942.2 F g^{-1}	
				5 A g^{-1}	930.0 F g^{-1}	
				10 A g^{-1}	923.3 F g^{-1}	
$NiCo_2S_4$ Nanosheets	NF	3 M KOH	1	1 A g^{-1}	744 F g^{-1}	15
				2 A g^{-1}	736 F g^{-1}	
				5 A g^{-1}	710 F g^{-1}	
				10 A g^{-1}	674 F g^{-1}	
				20 A g^{-1}	620 F g^{-1}	
				50 A g^{-1}	528 F g^{-1}	
$NiCo_2S_4$ urchin-like nanostructures	NF	6 M KOH	2-3	1 A g^{-1}	1149 F g^{-1}	16
				2 A g^{-1}	1056 F g^{-1}	
				3 A g^{-1}	1065 F g^{-1}	
				4 A g^{-1}	1062 F g^{-1}	
				5 A g^{-1}	1056 F g^{-1}	
				7 A g^{-1}	1032 F g^{-1}	
				10 A g^{-1}	1018 F g^{-1}	
$NiCo_2S_4$ nanotube	CC	3 M KOH	--	1 mA cm^{-2}	3.9 F cm^{-2}	17
Ni/Co-LDH@$NiCo_2S_4$@G	NF	3 M KOH	51.0	1 A g^{-1}	2001.2 F g^{-1}	18
$NiCo_2S_4$ nanorod	NF	1 M KOH	5	5 mA cm^{-2}	494 F g^{-1}	19
$NiCo_2S_4$ nanoflakes	NF	3 M KOH	0.2	5 mA cm^{-2}	1076 F g^{-1}	20
Ni_3S_2/$CoNi_2S_4$ nanosheets	NF	6 M KOH	--	2 A g^{-1}	2435 F g^{-1}	21
				3 A g^{-1}	2414 F g^{-1}	
				5 A g^{-1}	2340 F g^{-1}	
				10 A g^{-1}	2174 F g^{-1}	
				15 A g^{-1}	2040 F g^{-1}	
				20 A g^{-1}	1940 F g^{-1}	
				30 A g^{-1}	1752 F g^{-1}	
				40 A g^{-1}	1440 F g^{-1}	
$NiCo_2S_4$/Co_9S_8 submicro-spindles	NF	6 M KOH	5	4 A g^{-1}	749F g^{-1}	22
				15 A g^{-1}	620 F g^{-1}	
MCo_2S_4 (M = Ni, Fe, Zn) nanotubes	NF	3 M KOH	--	1 A g^{-1}	1780 F g^{-1}	23

Table S4. The distance (d_{Ni-O}) of OH on Ni_3S_2(001) and Co-Ni_3S_2(001), and the length of Ni-S band.

	d_{Ni-O}/Å	d_{Ni-S} /Å
Ni_3S_2(001)	1.88	2.29
Co-Ni_3S_2(001) Ni site	1.84	2.21
Co-Ni_3S_2(001) Co site	1.83	2.21

Table S5. The calculated specific capacity (Q_m), specific capacitance (C_m), energy density (E) and power density (P) of the Co-Ni_3S_2/NF//AC/NF device.

Current density/A g^{-1}	Q_m/ mAh g^{-1}	Discharge time/s	C_m/F g^{-1}	E/Wh kg^{-1}	P/kW kg^{-1}
5	308	222	695	246	3.99
10	294	106	663	236	8.01
15	267	63.6	596	212	12.0
20	222	40.3	504	179	16.0
30	200	23.8	446	159	24.0
40	178	15.3	383	136	32.0

Reference

1 D. Du, R. Lan, W. Xu, R. Beanland, H. Wang and S. Tao, *J. Mater. Chem. A*, 2016, **4**, 17749-17756.

2 Q. Zhou, J. Xing, Y. Gao, X. Lv, Y. He, Z. Guo and Y. Li, *ACS Appli. Mater. Interf.*, 2014, **6**, 11394-11402.

3 R. Li, S. Wang, Z. Huang, F. Lu and T. He, *J. Power Sources*, 2016, **312**, 156-164.

4 C. Wang, K. Guo, W. He, X. Deng, P. Hou, F. Zhuge, X. Xu and T. Zhai, *Sci. Bull.,* 2017, **62**, 1122-1131.

5 T.-W. Lin, M.-C. Hsiao, S.-W. Chou, H.-H. Shen and J.-Y. Lin, *J. Electrochem. Soci.*, 2015, **162**, A1493-A1499.

6 J. K. Norskov, J. Rossmeisl, A. Logadottir, L. Lindqvist, J. R. Kitchin, T. Bligaard and H. Jonsson, *J. Phys. Chem. B*, 2004, **108**, 17886-17892.

7 F. Wang, T. Wen, X. Lv, H. Zhang, Z. Hu, Y. Zhang, J. Ji and W. Jiang, *J. Mater. Chem. A*, 2018,**6**, 10490-10496.

8 J. Xiao, L. Wan, S. Yang, F. Xiao and S. Wang, *Nano Lett.*, 2014, **14**, 831-838.

9 W. Du, Z. Wang, Z. Zhu, S. Hu, X. Zhu, Y. Shi, H. Pang and X. Qian, *J. Mater. Chem. A*, 2014, **2**, 9613.

10 Y. Zhang, M. Ma, J. Yang, C. Sun, H. Su, W. Huang and X. Dong, *Nanoscale*, 2014, **6**, 9824-9830.

11 W. Fu, C. Zhao, W. Han, Y. Liu, H. Zhao, Y. Ma and E. Xie, *J. Mater. Chem. A*, 2015, **3**, 10492-10497.

12 W. Zeng, G. Zhang, X. Wu, K. Zhang, H. Zhang, S. Hou, C. Li, T. Wang and H. Duan, *J. Mater. Chem. A*, 2015, **3**, 24033-24040.

13 Y. Zhu, Z. Wu, M. Jing, X. Yang, W. Song and X. Ji, *J. Power Sources*, 2015, **273**, 584-590.

14 J. Yang, W. Guo, D. Li, Q. Qin, J. Zhang, C. Wei, H. Fan, L. Wu and W. Zheng, *Electrochim. Acta*, 2014, **144**, 16-21.

15 Z. Wu, X. Pu, X. Ji, Y. Zhu, M. Jing, Q. Chen and F. Jiao, *Electrochimi. Acta*, 2015, **174**, 238-245.

16 H. Chen, J. Jiang, L. Zhang, H. Wan, T. Qi and D. Xia, *Nanoscale*, 2013, **5**, 8879-8883.

17 R. Ding, M. Zhang, Y. Yao and H. Gao, *J. Colloid Inter. Sci.*, 2016, **467**, 140-147.

18 Y. Tao, L. Ruiyi, Z. Lin, M. Chenyang and L. Zaijun, *Electrochim. Acta*, 2015, **176**, 1153-1164.

19 T. Xiao, J. Li, X. Zhuang, W. Zhang, S. Wang, X. Chen, P. Xiang, L. Jiang and X. Tan, *Electrochim. Acta*, 2018, **269**, 397-404.

20 S. K. Shinde, M. B. Jalak, G. S. Ghodake, N. C. Maile, V. S. Kumbhar, D. S. Lee, V. J. Fulari and D. Y. Kim, *Appl. Surf. Sci.*, 2019, **466**, 822-829.

21 W. He, C. Wang, H. Li, X. Deng, X. Xu and T. Zhai, *Adv. Energy Mater.*, 2017, **7**, 1700983.

22 L. Hou, Y. Shi, S. Zhu, M. Rehan, G. Pang, X. Zhang and C. Yuan, *J. Mater. Chem. A*, 2017, **5**, 133-144.

23 J. Wu, X. Shi, W. Song, H. Ren, C. Tan, S. Tang and X. Meng, *Nano Energy*, 2018, **45**, 439-447.